



# Influence of the microstructure on the corrosion behaviour of a shape memory Cu–Al–Be alloy in a marine environment

S. Montecinos<sup>a,b,\*</sup>, S.N. Simison<sup>a,b</sup>

<sup>a</sup> INTEMA, Facultad de Ingeniería, Universidad Nacional de Mar del Plata, Juan B. Justo 4302, (7600) Mar del Plata, Argentina

<sup>b</sup> CONICET, Argentina

## ARTICLE INFO

### Article history:

Received 1 September 2010

Received in revised form 13 October 2010

Accepted 13 October 2010

Available online 20 October 2010

### Keywords:

Copper-based alloys

Corrosion

Microstructure

Shape memory alloys

## ABSTRACT

The influence of the microstructure on the corrosion behaviour of a shape memory Cu–11.40Al–0.55Be (wt.%) polycrystalline alloy in 3.5% NaCl has been studied by microscopical examinations, spectroscopical and X-ray diffraction measurements, and electrochemical tests. Chloride environment can produce a dealuminization attack, and the corrosion behaviour is affected by the alloy microstructural conditions. After long times of immersion, the single  $\beta$  phase microstructure suffers localized corrosion in some regions but dealuminization is generalized on the whole surface. However, in the ( $\beta + \gamma_2$ ) microstructure, preferential dissolution of  $\gamma_2$  dendritic precipitates occurs, which seems to protect  $\beta$  matrix from dealloying.

© 2010 Elsevier B.V. All rights reserved.

## 1. Introduction

Copper alloys are widely used in marine environments because of their low corrosion susceptibility. The corrosion of copper and its alloys has been extensively studied in chloride media where it has been observed that the chloride ion has a strong influence on the copper corrosion mechanism. The corrosion resistance of aluminium bronzes has been attributed to the effect of aluminium, which improves the quality of the reaction product film and renders it more protective. However, some researchers attributed the protection to the formation of an  $\text{Al}_2\text{O}_3$  film, while others attributed it to the doping of the  $\text{Cu}_2\text{O}$  film with aluminium ions [1–7]. In oxygenated seawater,  $\text{Cu}_2\text{O}$  is generally oxidised over time to cupric hydroxide ( $\text{Cu}(\text{OH})_2$ ), atacamite ( $\text{Cu}(\text{OH})_3\text{Cl}$ ) or malachite ( $\text{CuCO}_3 \cdot \text{Cu}(\text{OH})_2$ ) [8].

Dealloying is a corrosion process in which one constituent of an alloy is preferentially removed, leaving behind an altered residual structure. This process has been reported in a number of copper-based alloy systems. Two theories are most prevalent to clarify the dealloying mechanisms [4,5,9]. In the first one, two metals in an alloy are dissolved, and one redeposits on the surface. In the second theory, one metal is selectively dissolved from an alloy, leaving a porous residue of the more noble species. In certain corrosive

environments, aluminium bronzes can suffer a selective corrosion attack known as dealuminization. This selective attack results in a loss of aluminium from the alloy. It has been also demonstrated that the hypereutectoid martensite and the  $\gamma$  phase are more susceptible to dealuminization than the matrix [4,5]. So, the microstructure of the alloy will be determinant in its corrosion resistance.

Previous results on Cu–11.4Al (wt.%) alloys with the addition of small amounts of Be have demonstrated that they exhibit the pseudoelastic behaviour at room temperature [10–16]. Applying mechanical stress to the  $\beta$  phase, 18R martensite is induced ( $\beta'$ ), resulting in a macroscopical change of shape. Under appropriate conditions, a hysteretic loop is formed when removing the load, and the strain is almost fully recovered. For that reason, the use of Cu–Al–Be alloys is highly promising for applications as passive dampers of seismic energy [13,15]. Studies about the thermomechanical behaviour of these alloys have been performed [14–16]. Nevertheless, an analysis of their corrosion behaviour in view of their application in bridges as seismic dampers is still missing. Under slow cooling from high temperature, the formation of the proeutectoid  $\gamma_2$  phase can be produced [17–19]. The shape memory properties can be modified, among other several factors, by the presence of these precipitates [20]. However, their influence on the possible formation of localized corrosion in these alloys has not been reported yet.

In the present study we analyzed the influence of the microstructure on the corrosion behaviour of a shape memory Cu–Al–Be alloy in 3.5% NaCl in view of its application in bridges as seismic dampers.

\* Corresponding author at: INTEMA, Facultad de Ingeniería, Universidad Nacional de Mar del Plata, Juan B. Justo 4302, (7600) Mar del Plata, Argentina.

E-mail address: [dmonteci@fi.mdp.edu.ar](mailto:dmonteci@fi.mdp.edu.ar) (S. Montecinos).

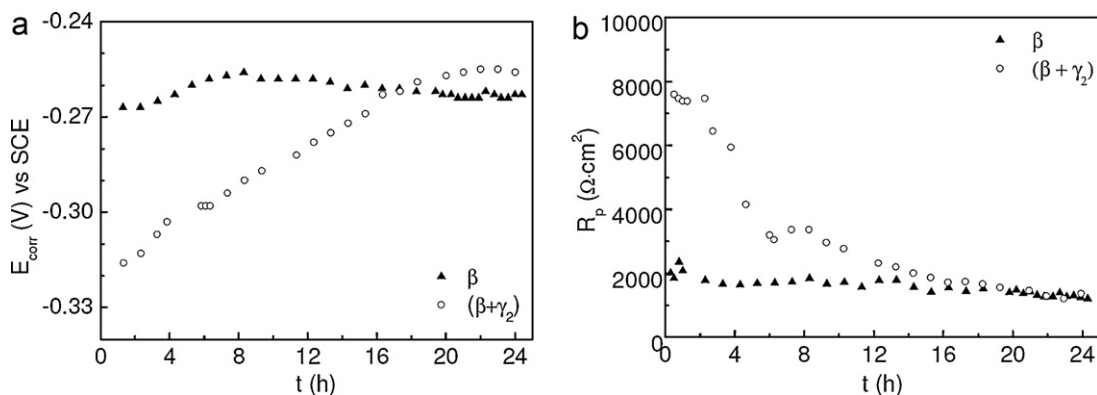


Fig. 1.  $E_{\text{corr}}$  (a) and  $R_p$  (b) for the  $\beta$  and  $(\beta + \gamma_2)$  microstructures in 3.5% NaCl as a function of immersion time.

## 2. Experimental procedure

The Cu–11.40Al–0.55Be (wt.%) polycrystalline alloy under study was obtained from Trefimetaux (France), as 15 mm diameter extruded bars. The chemical composition was determined by atomic absorption spectrophotometry. The nominal martensitic transformation starting temperature,  $M_s$ , is 217 K [10]. Samples with two different microstructures were employed: single  $\beta$  phase and  $\beta$  matrix with  $\gamma_2$  dendritic precipitates. Prior to performing the heat treatments, the samples were heated during 5 min at 1073 K in the  $\beta$  field and water quenching at room temperature (single  $\beta$  phase microstructure). Precipitation of dendritic  $\gamma_2$  phase was generated by slow cooling at 1.3 K/min from 1073 K to 808 K, followed by water quenching at room temperature ( $\beta$  phase with  $\gamma_2$  precipitates microstructure). A detailed description is given in [17]. The temperature was monitored using a chromel–alumel thermocouple spot welded to the sample. A volume fraction of the  $\gamma_2$  phase of  $13.7 \pm 1.2\%$  was estimated from optical micrographs as the relative area occupied by the precipitates with respect to the total area using the software Image Tool 3.0. The samples were smoothed with 240, 600 and 1000 grit emery paper and then polished with alumina powder (0.3  $\mu\text{m}$  size).

Specimens with both microstructures were immersed in a 3.5% NaCl solution adjusted to pH 8 with borate–boric acid buffer for different exposure times in the range of 10 min to 40 days. The solution was maintained at room temperature, and air was bubbled through it.

The surface morphology of the samples before and after the immersion was examined using an Olympus PMG3 optical microscope (OM) and a JEOL JSM-6460LV scanning electron microscope (SEM). Energy dispersive X-ray spectroscopy (EDX) analysis under SEM was employed to estimate the surface composition of different regions of the samples. The errors were determined as the standard deviation of the at least three measurements. Corrosion products after 24 h of immersion at open circuit potential ( $E_{\text{corr}}$ ) were locally characterized by micro-Raman spectroscopy (Invia Reflex confocal Raman Microprobe). The incident beam was focused on the specimens as a spot size diameter of 10  $\mu\text{m}$  (standard mode) and 1  $\mu\text{m}$  (confocal mode). Excitation was provided with the 514 nm emission line of an Ar<sup>+</sup> laser and measurements were performed in backscattering configuration using a 50 $\times$  objective. X-ray diffraction (XRD) using a PANanalytical X'Pert Pro PW3373 equipment with normal and low incidence angle (3 $^\circ$ ) was used to identify the phase structure of specimens before the immersion and of the corrosion product films formed after that. It was operated at 40 kV and 40 mA with the excitation of CuK $\alpha$  ( $\lambda = 1.54056 \text{ \AA}$ ). Tapping mode atomic force microscopy (AFM) using an Agilent 5500 microscope was employed to study “*in-situ*” the changes in the topography of

the sample surfaces immersed in 3.5% NaCl during the first two and a half hours.

Electrochemical tests were conducted using a conventional three electrode cell of 150 mL volume. The potentials were measured against a saturated calomel electrode (SCE). A platinum wire was used as counterelectrode. The working electrodes were made of cylindrical pieces of around 5.4 mm diameter, mounted with fast curing epoxy resin on appropriate holders of PVC. The exposed area of the electrodes was 0.23 cm<sup>2</sup>. Prior to the electrochemical tests, the electrode surface was smoothed with 240, 600 and 1000 grit emery paper. Measurements of open circuit potential ( $E_{\text{corr}}$ ) and linear polarization resistance ( $R_p$ ) during 24 h of immersion were performed to obtain some information about the evolution of the corrosion process. Polarization curves were measured potentiodynamically at a scan rate of 0.1 mV s<sup>−1</sup> using a Voltalab (PGZ 402) potentiostat. For each measure, the electrodes were maintained at open circuit during at least 10 min, for stabilization, and  $E_{\text{corr}}$  was obtained. The linear polarization method was used for the determination of the polarization resistance ( $R_p$ ) of the electrodes for different immersion times. Polarizations of  $\pm 15 \text{ mV}$  from  $E_{\text{corr}}$  were used. The slope of the tangent at the origin provided the value of  $R_p$ .

## 3. Results

### 3.1. Electrochemical tests

Fig. 1a illustrates the open-circuit potential as a function of immersion time during 24 h for the  $\beta$  and  $(\beta + \gamma_2)$  microstructures in 3.5% NaCl. Data obtained for each microstructure are reproducible with an error smaller than 10 mV. As can be seen, after 3 h of immersion  $\beta$  sample reached a steady state, with a final potential of  $\sim -0.26 \text{ V}$ . The sample with  $\gamma_2$  precipitates presented an increase of the open circuit potential, and a steady state was reached after 16 h from immersion, with a final potential similar to that of the single phase microstructure. The polarization resistance data exhibited a similar behaviour (Fig. 1b). The single phase microstructure reached a value of  $R_p \sim 1500 \Omega \text{cm}^2$  from 3 h of immersion onwards. Using the Tafel slopes reported for Cu–Al alloys in the range 8–13 wt.% Al for both regions, anodic (60 mV decade<sup>−1</sup>) and cathodic (120 mV decade<sup>−1</sup>) [8,21], a corrosion current of 12  $\mu\text{A}/\text{cm}^2$  (0.12 mm/year) could be estimated. The corrosion current was lower for the sample with precipitates for short periods of exposure ( $\sim 2.3 \mu\text{A}/\text{cm}^2$  or 0.02 mm/year), and increased with the immersion time, reaching a similar value to that of the single phase microstructure after 24 h of immersion.

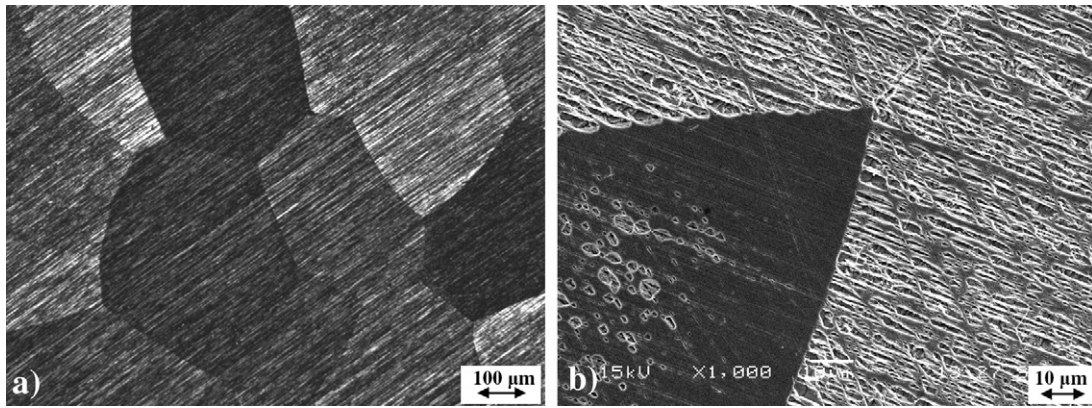


Fig. 2.  $\beta$  sample immersed for a period of 24 h in 3.5% NaCl (OM and SEM).

Table 1

EDX analysis of  $\beta$  sample before and after 24 h of immersion in 3.5% NaCl.

Element	Mass concentration (wt.%)		
	Before immersion	24 h bright grain	24 h dark grain
Cu	88.0 $\pm$ 0.2	86.7 $\pm$ 0.2	87.6 $\pm$ 0.8
Al	12.0 $\pm$ 0.2	11.0 $\pm$ 0.1	11.3 $\pm$ 0.7
O		2.2 $\pm$ 0.1	0.9 $\pm$ 0.01
Cl		0.1 $\pm$ 0.01	0.2 $\pm$ 0.01

### 3.2. Surface characterization

#### 3.2.1. Single $\beta$ phase microstructure

Fig. 2 showed the surface of the  $\beta$  phase samples obtained after 24 h of immersion in 3.5% NaCl by OM and SEM. Grains were revealing by the corrosion process. The EDX and micro-Raman analysis results of different grains are given in Tables 1 and 2. The peaks of micro-Raman vibrational data were assigned to the surface species according to data reported in the literature. It is important to consider that the data reported by different authors present slight variations in the position of the peaks for the same chemical species. Before immersion, the specimen presented almost the same composition in different zones (the Be content could not be detected

by EDX measurements). After 24 h of immersion, the aluminium content of the surface was slightly lower, and corrosion products containing O and Cl were formed on top of the samples (Table 1). The presence of CuO, Cu<sub>2</sub>O and CuCl<sub>2</sub> was identified by micro-Raman (Table 2). Higher concentrations of O and greater intensities of the vibrational data peaks were found in the bright grains than those for the dark ones. It suggests the presence of thicker layers of corrosion products in the bright grains. Small quantities of C were also detected by EDX, which was attributed to the formation of malachite from the micro-Raman measurements.

The diffraction patterns of the specimen before immersion confirmed the DO<sub>3</sub> structure of  $\beta$  Cu–Al–Be alloy ( $a=5.77$  Å), and revealed the presence of some martensite phase,  $\beta'$  ( $a=4.49$  Å,  $b=5.19$  Å,  $c=46.61$  Å) (Fig. 3a). The patterns of the corrosion products formed on the sample after 24 h of immersion indicated the existence of CuO and Cu<sub>2</sub>O (Fig. 3b). These results are in agreement with EDX and micro-Raman measurements. Other authors have found that when a copper surface is heated in air, oxygen or water, a duplex film forms where the primary component is Cu<sub>2</sub>O with a lower concentration of CuO and/or Cu(OH)<sub>2</sub> [8].

After 40 days of immersion, localized corrosion could be observed in the surface of the sample (Fig. 4). The EDX analysis results of different morphological zones are given in Table 3.

Table 2

Micro-Raman vibrational data of surface species in the  $\beta$  sample after 24 h of immersion in 3.5% NaCl (w: weak; m: middle; s: strong).

	Frequency shift (cm <sup>-1</sup> )			
	Cu <sub>2</sub> O [22–24]	CuO [22–24]	CuCO <sub>3</sub> ·Cu(OH) <sub>2</sub> [24]	CuCl <sub>2</sub> [24]
Bright grain	154w, 644s, 785s, 868m	540m, 1013s	430m, 752w	288s
Dark grain	147w, 644s, 868m	540m	430m, 759w	288s

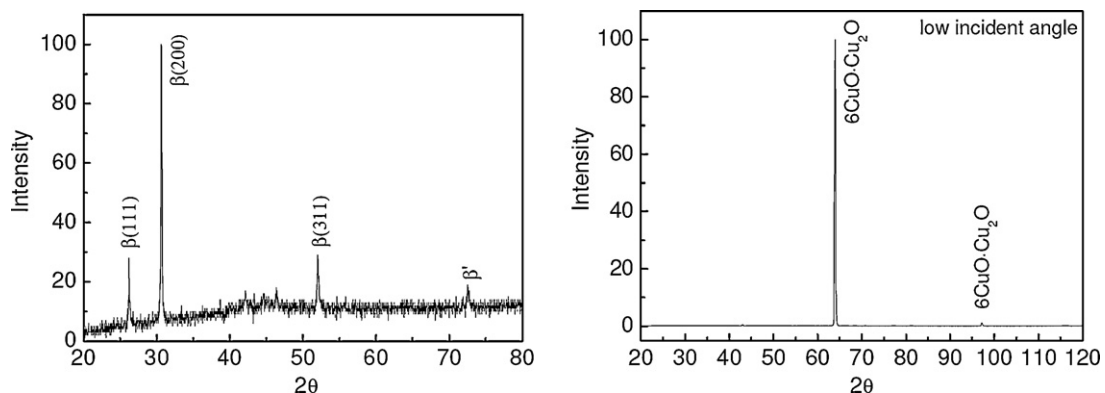


Fig. 3. XRD patterns of the  $\beta$  sample (a) before and (b) after 24 h of immersion in 3.5% NaCl. The last one was obtained at low incidence angle ( $3^\circ$ ).

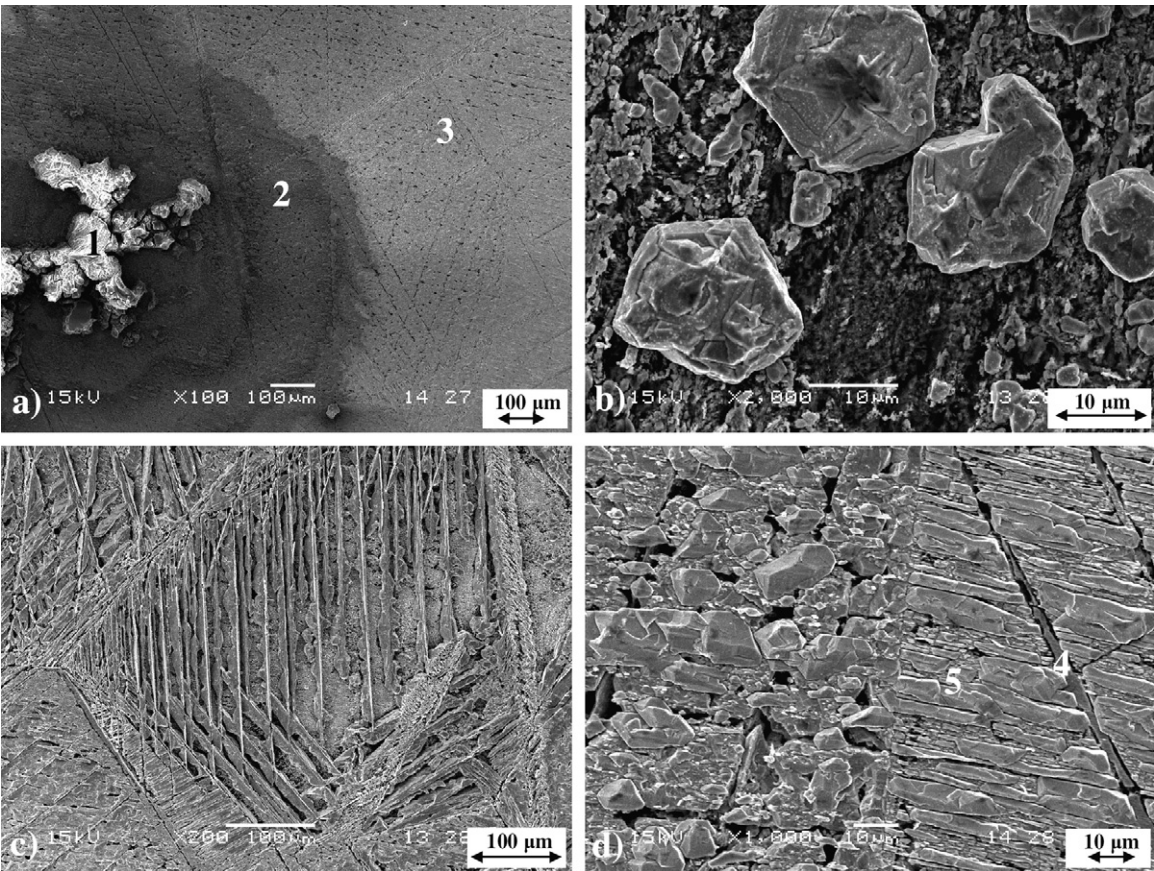


Fig. 4.  $\beta$  sample immersed for a period of 40 days in 3.5% NaCl (SEM).

**Table 3**  
EDX analysis of  $\beta$  sample after 40 days of immersion in 3.5% NaCl.

Element	Mass concentration (wt.%)		
	Zone 1	Zone 2	Zone 3
Cu	2.1 ± 0.1	29.4 ± 1.5	96.5 ± 0.9
Al	31.4 ± 1.6	0.7 ± 0.01	0.8 ± 0.1
O	58.7 ± 2.9	1.2 ± 0.1	2.5 ± 0.6
Cl	7.5 ± 0.4	30.1 ± 1.5	0.2 ± 0.2
Na	0.3 ± 0.01	38.7 ± 1.9	0.00

Zone 1 in Fig. 4a is rich in O and Al. In some zones of the sample where this corrosion product was absent, particles of Cu could be observed (Fig. 4b). The copper content of these zones was as high as 97.2 wt.%. Consequently it can be deduced that the dealumina-

tion of the alloy and the presence of copper crystals could point to a dissolution–redeposition mechanism [7,9].

In zone 2 in Fig. 4a the presence of NaCl and corrosion products based on O were detected. The matrix far from zone 1 (zone 3) was also rich in Cu and impoverished in Al. A particular pattern caused by dealumination could be observed (Fig. 4c and d) with almost uncorroded parallel regions (zone 4 in Fig. 4d), which have different orientations in each grain. The area between these parallel regions (zone 5 in Fig. 4d) was depleted in aluminium, with copper content as high as 97.9 wt.%. From Fig. 4c and d, it could be inferred that the presence of copper was produced by the selective dissolution of aluminium from the alloy, leaving a porous matrix.

The diffraction patterns of the specimen after 25 days of immersion (Fig. 5a) confirmed the existence of CuO, Cu<sub>2</sub>O, and Al<sub>2</sub>O<sub>3</sub> in the surface of the sample. These results suggested that the zone 1

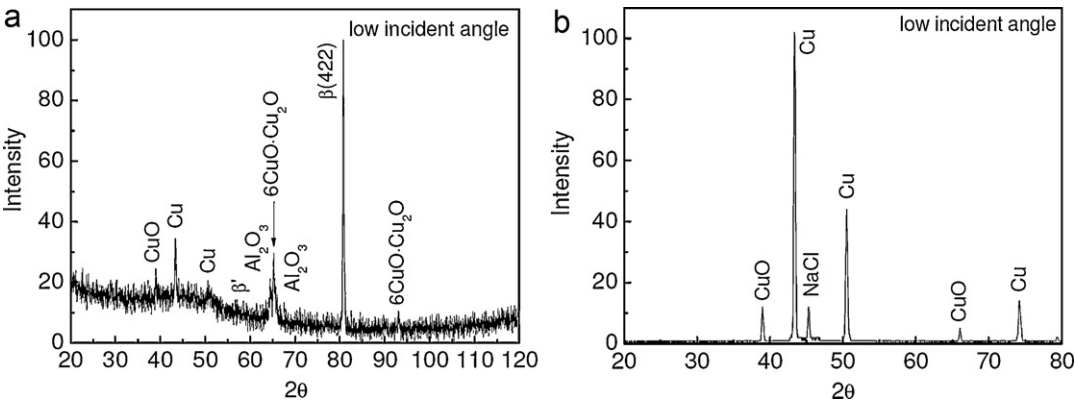


Fig. 5. XRD pattern of the  $\beta$  sample after 25 days (a) and 40 days (b) of immersion in 3.5% NaCl obtained at low incidence angle ( $3^\circ$ ).

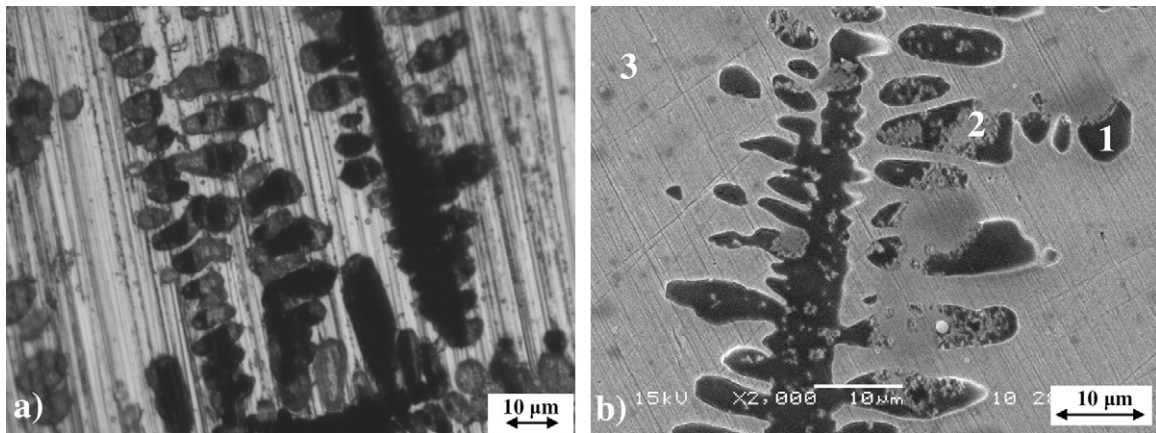


Fig. 6. ( $\beta + \gamma_2$ ) sample immersed for a period of 24 h in 3.5% NaCl (OM and SEM).

in Fig. 4a would correspond to  $\text{Al}_2\text{O}_3$ . After 40 days of immersion a notable presence of copper was observed (Fig. 5b).

### 3.2.2. Two-phases ( $\beta + \gamma_2$ ) microstructure

Fig. 6 shows the surface of the ( $\beta + \gamma_2$ ) sample obtained after 24 h of immersion in 3.5% NaCl. The precipitates could be clearly seen, some of them were completely dark, others were not. The EDX and micro-Raman analysis results from different morphological zones are given in Tables 4 and 5. Measurements of the matrix were done at a distance of  $\sim 10 \mu\text{m}$  from the precipitates. The  $\gamma_2$  precipitates were rich in Al, as has been reported previously for a similar alloy [25]. After 24 h of immersion, a surface film rich in O and Al formed on the precipitates, which would correspond to  $\text{Al}_2\text{O}_3$ , as was identified by micro-Raman (Table 5). Cl and small quantities of C were also detected by EDX, which were associated to the presence of  $\text{CuCl}_2$ ,  $\text{CuCl}$  and malachite (Table 5). The matrix was impoverished in Al, and contains some corrosion products (Table 4). The presence of  $\text{CuO}$ ,  $\text{Cu}_2\text{O}$ ,  $\text{CuCl}_2$ , and malachite were identified by micro-Raman on the matrix and on the precipitates (Table 5).

The diffraction patterns of the specimen before immersion confirmed the presence of precipitates  $\gamma_2$  with a  $\text{Cu}_9\text{Al}_4$  structure in a  $\beta$  matrix, and some martensite phase (Fig. 7a). Martensite phase was also observed by OM at room temperature. The formation of high volume fractions of  $\gamma_2$  precipitates decreased the aluminium content in the matrix around them, therefore the temperature  $M_s$  of these zones increased [20]. The XRD patterns after 24 h of immersion corroborated the presence of  $\text{Al}_2\text{O}_3 \cdot \text{H}_2\text{O}$  in the surface of the specimen (Fig. 7b). The existence of  $\text{CuO}$ ,  $\text{Cu}_2\text{O}$  and malachite in the corrosion products was also identified.

Table 4  
EDX analysis of ( $\beta + \gamma_2$ ) sample before and after 24 h of immersion in 3.5% NaCl.

Element	Mass concentration (wt.%)				
	before immersion		after immersion		
	$\gamma_2$	Matrix	Dark $\gamma_2$ (1)	Partially dark $\gamma_2$ (2)	Matrix (3)
Cu	$84.4 \pm 0.9$	$88.3 \pm 0.4$	$45.8 \pm 5.0$	$74.8 \pm 5.9$	$81.3 \pm 3.5$
Al	$15.6 \pm 0.9$	$11.7 \pm 0.4$	$17.8 \pm 3.2$	$13.8 \pm 1.0$	$8.9 \pm 1.1$
O			$35.7 \pm 8.4$	$9.9 \pm 5.8$	$9.7 \pm 4.6$
Cl			$0.7 \pm 0.2$	$0.3 \pm 0.1$	$0.2 \pm 0.1$

Table 5  
Confocal micro-Raman vibrational data of surface species in the ( $\beta + \gamma_2$ ) sample after 24 h of immersion in 3.5% NaCl (w: weak; m: middle; s: strong).

	Frequency shift ( $\text{cm}^{-1}$ )					
	$\text{Cu}_2\text{O}$ [22–24]	$\text{CuO}$ [22–24]	$\text{CuCO}_3 \cdot \text{Cu}(\text{OH})_2$ [24]	$\text{CuCl}_2$ [24]	$\text{CuCl}$ [24]	$\text{Al}_2\text{O}_3$ [24]
Matrix	146w, 220w, 644s, 786w, 880m	540w, 720w, 1012s	433w	290s		
Dark $\gamma_2$	146w, 526w, 786w	342m, 720w	433w	290s	206s, 262s	620s

Table 6  
EDX analysis of ( $\beta + \gamma_2$ ) microstructure after 34 days of immersion in 3.5% NaCl.

Element	Mass concentration (wt.%)		
	Matrix	Zone 1	Zone 2
Cu	$85.3 \pm 0.1$	$97.0 \pm 2.3$	$88.5 \pm 5.2$
Al	$11.9 \pm 0.1$	$0.4 \pm 0.2$	$5.5 \pm 3.5$
O	$2.8 \pm 0.1$	$2.5 \pm 2.1$	$5.6 \pm 1.6$
Cl	$0.1 \pm 0.01$	$0.2 \pm 0.01$	$0.7 \pm 0.2$

The variation in the topography of the sample surfaces at an early stage was evaluated “*in-situ*” by AFM. Fig. 8 shows three sequential images ( $50 \mu\text{m} \times 50 \mu\text{m}$ ) of a surface that has been exposed to 3.5% NaCl for 30, 120 and 160 min. The image at the top is a 3D view of topography data and the one at the bottom is the phase image corresponding to each one. Phase image is the mapping of the changes in the phase angle of the cantilever oscillation during the tapping mode scan, and contrast variations in this image can be associated to changes in the properties of the sample surface [26]. Consequently, the increase in contrast of the precipitates with time of exposure (Fig. 8) could be related to the formation of a new compound with a different composition.

After 34 days of immersion, localized corrosion occurs in the precipitates zones (Fig. 9). The  $\text{Al}_2\text{O}_3$  film cannot be seen and a different morphology deposit, with copper content as high as 97.0 wt.%, was identified by EDX (zone 1 in Table 6). This copper rich layer appeared covering completely some of the precipitates (Fig. 9a), while its presence could not be detected on others (Fig. 9a and b). In those precipitates where the copper rich deposit seems to

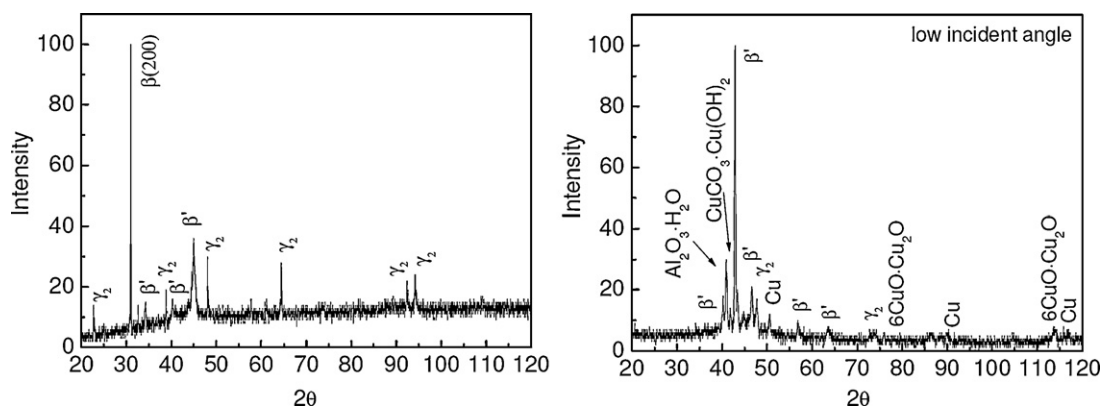


Fig. 7. XRD patterns of the ( $\beta + \gamma_2$ ) sample (a) before and (b) after 24 h of immersion in 3.5% NaCl. The last one was obtained at low incidence angle ( $3^\circ$ ).

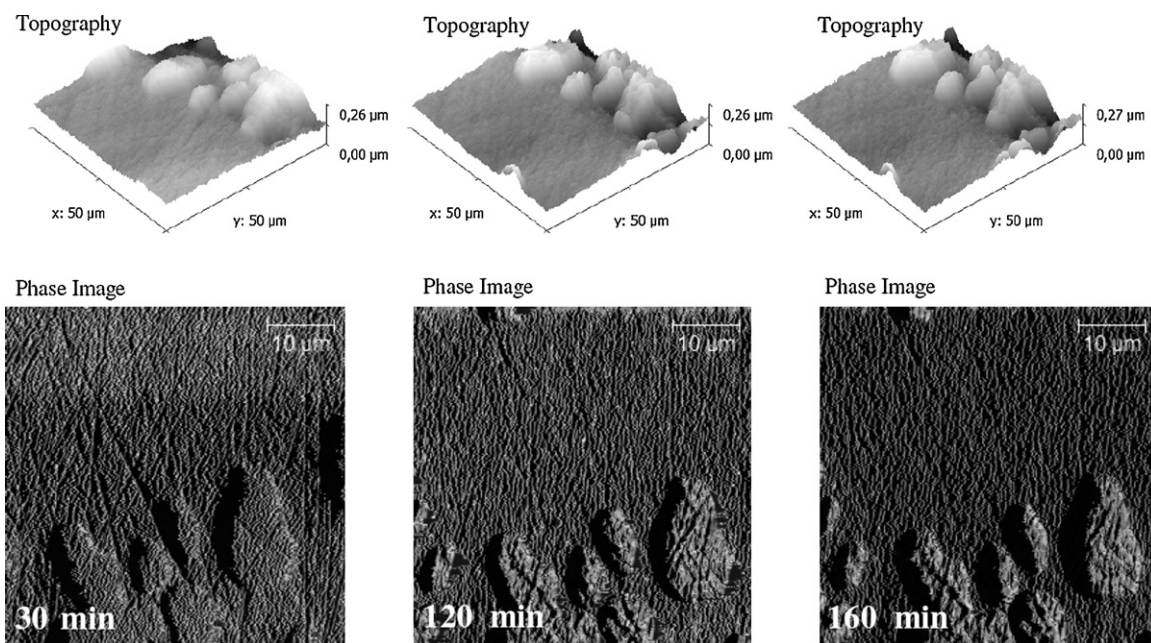


Fig. 8. In-situ AFM images in 3.5% NaCl of ( $\beta + \gamma_2$ ) microstructure for various immersion times. The 3D topography and the phase image for each time are shown.

have been detached, a porous product could be observed. This product was impoverished in aluminium and contains O and Cl (zone 2 in Table 6). Small quantities of C were also detected by EDX in all the analyzed zones.

The diffraction patterns of the specimen after 25 days of immersion confirmed the existence of  $\text{Al}_2\text{O}_3 \cdot \text{H}_2\text{O}$ ,  $\text{Cu}_2\text{O}$ ,  $\text{CuO}$ , malachite,  $\text{CuCl}$  and  $\text{CuCl}_2$  in the surface of the sample. Cu was also identified.

After 34 days of immersion the presence of  $\text{CuO}$  and  $\text{Cu}$ , and the absence of  $\text{Al}_2\text{O}_3$  were confirmed (Fig. 10).

#### 4. Discussion

The pseudoelastic behaviour of Cu–Al alloys strongly depends on chemical composition and microstructure. The Cu–Al system

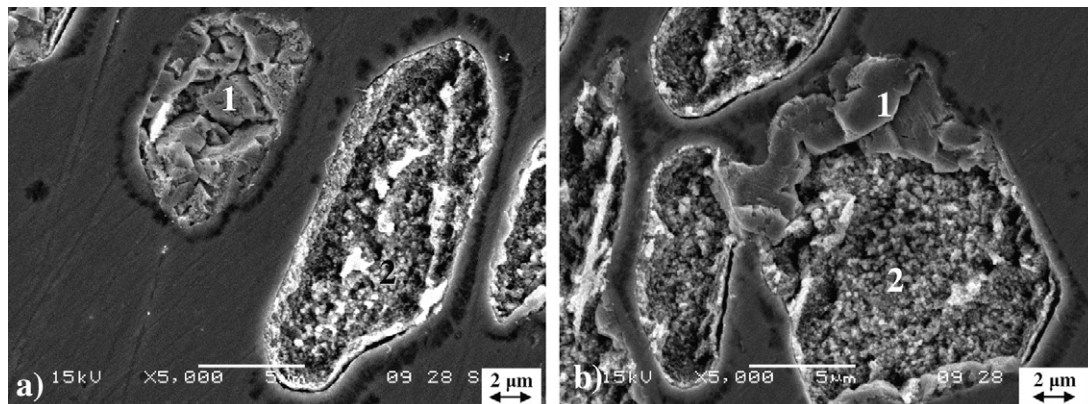


Fig. 9. ( $\beta + \gamma_2$ ) microstructure immersed for a period of 34 days in 3.5% NaCl (SEM).

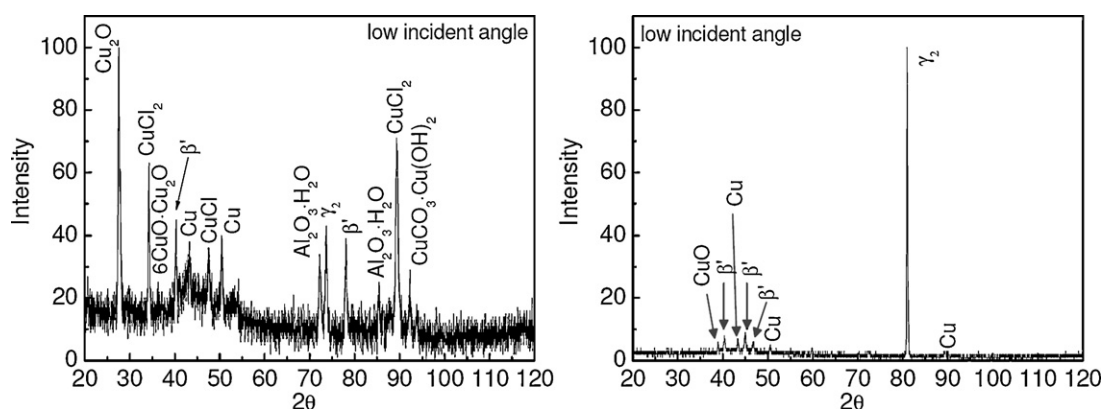
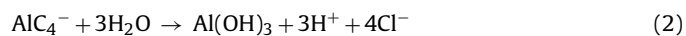


Fig. 10. XRD pattern of the ( $\beta + \gamma_2$ ) sample after 25 days (a) and 34 days (b) of immersion in 3.5% NaCl obtained at low incidence angle ( $3^\circ$ ).

exhibits shape memory properties only in the range of 11–12 wt.% Al approximately [18]. A decrease in the Al content results in an increase of  $M_s$  of  $-71$  K each 1 wt.% [10]. Regarding microstructure, the influence of  $\gamma_2$  precipitates on the martensitic transformation of a Cu–11.41Al–0.50Be (wt.%) polycrystalline alloy has been previously studied [20]. It was shown that the increase in the precipitate content (or size) deteriorates the pseudoelastic response and the stress-induced martensitic transformation occurs at higher stress levels respect to the single  $\beta$  phase microstructure. For application of these alloys in bridges as passive dampers of seismic energy, it is important to understand the effect of the marine environment on the alloy, and how it could influence on the pseudoelastic behaviour. In the present work, a characterization of the corrosion products which form on the studied Cu–Al–Be alloy and their evolution with exposure time was developed.

After 24 h of immersion, a  $\text{Cu}_2\text{O}/\text{CuO}$  surface film is formed on the  $\beta$  matrix for both microstructures. Early investigations of copper in chloride media have found that the initial corrosion product of copper is cuprous chloride,  $\text{CuCl}$ , which reacts to produce cuprous oxide,  $\text{Cu}_2\text{O}$ , and the subsequent oxidation to  $\text{CuO}$  at higher potential [8]. It was found that after long times of immersion, the stable corrosion product was  $\text{CuO}$  and the presence of  $\text{Cu}_2\text{O}$  was not detected. The results also revealed that aluminium oxide was present only at short times of immersion, and it was not found after long times, which would indicate that its presence is not necessary to assure the stability of the protective films.

The formation of the aluminium hydrated oxide/hydroxide could be due to the complexation of aluminium by chloride, followed by hydrolysis [4,7]:



After long times of immersion, the single  $\beta$  phase microstructure suffered localized corrosion in some regions but dealuminization is generalized on the whole surface (Table 3). However, the  $\beta$  matrix in the two phases microstructure remained almost unaltered, while the  $\gamma_2$  precipitates corroded preferentially (Table 6). As these precipitates have higher aluminium content, they will also have a stronger tendency to preferential dealuminization.  $\gamma_2$  precipitates would cathodically protect  $\beta$  matrix while undergoing a loss of aluminium by selective-dissolution. Although the matrix could display a compositional profile close to the precipitates, localized corrosion was not observed.

Since pseudoelastic behaviour is highly dependent on Al and Be content in the matrix, dealloying should be avoided regarding applications as passive dampers in corrosive environments. The apparent beneficial effect of precipitates on the chemical stability of the matrix should be characterized in greater depth. Unfortunately,

the presence of Be could not be detected by any of the experimental techniques employed (EDX, XRD, and micro-Raman). However, it is important to take into account that small changes in the Be content of the matrix strongly modify the temperature  $M_s$ .

More work is needed in order to evaluate the effect of corrosion (dealloyed layers vs. preferential precipitates dissolution) on the pseudoelastic behaviour of these alloys. Mechanical testing on corroded samples is in progress.

## 5. Conclusions

The corrosion behaviour of a shape memory Cu–11.40Al–0.55Be (wt.%) polycrystalline alloy in 3.5% NaCl has been characterized in view of its application in bridges as seismic dampers. Samples with two different microstructures were employed: single  $\beta$  phase and  $\beta$  matrix with  $\gamma_2$  dendritic precipitates. The following conclusions can be drawn:

- Chloride environment could produce a dealuminization attack on the studied alloy.
- The corrosion behaviour was affected by the alloy microstructural conditions.
- The single  $\beta$  phase microstructure suffered matrix dealloying (aluminium preferential dissolution) on the whole surface, with some zones where the localized corrosion attack was more severe.
- In the two-phase microstructure, preferential dissolution of  $\gamma_2$  dendritic precipitates occurred, which seems to protect  $\beta$  matrix from dealloying.
- For long exposure times only copper compounds were detected in the corrosion products.

The present results highlight the need of a systematic study on the effect of compositional profiles caused by dealloying in the pseudoelastic behaviour in order to clarify the suitability of these alloys for corrosive service.

## Acknowledgements

The authors acknowledge the financial support of the CONICET, and the University of Mar del Plata, Argentina.

## References

- H.E. El-Feky, N.H. Helal, M.R. Negem, Electrochemical behaviour of some copper alloys in sodium chloride solutions containing different inorganic additives, *J. Chem. Eng. Mater. Sci.* 1 (1) (2010) 8–22.
- E.A. Ashour, B.G. Ateya, Electrochemical behaviour of a copper–aluminium alloy in concentrated alkaline solutions, *Electrochim. Acta* 42 (2) (1997) 243–250.

- [3] H. Wojtas, S. Virtanen, H. Böhni, Electrochemical characterization of new stainless Cu–Al–Sn alloys, *Corros. Sci.* 37 (5) (1995) 793–799.
- [4] A.V. Benedetti, P.T.A. Sumodjo, K. Nobe, P.L. Cabot, W.G. Proud, Electrochemical studies of copper, copper–aluminium and copper–aluminium–silver alloys: Impedance results in 0.5 M NaCl, *Electrochim. Acta* 40 (16) (1995) 257–2668.
- [5] Z. Han, H. Zhao, Effect of  $\beta$  martensite transformation on dealuminification behaviour of Cu–9Al–2Mn alloy in a marine environment, *Mater. Sci. Eng. A* 345 (2003) 8–13.
- [6] Z. Han, Y.F. He, H.C. Lin, Dealloying characterizations of Cu–Al alloy in marine environment, *J. Mater. Sci. Lett.* 19 (2000) 393–395.
- [7] J.A. Wharton, K.R. Stokes, The influence of nickel–aluminium bronze microstructure and crevice solution on the initiation of crevice corrosion, *Electrochim. Acta* 53 (2008) 2463–2473.
- [8] G. Kear, B.D. Barker, F.C. Walsh, Electrochemical corrosion of unalloyed copper in chloride media—a critical review, *Corros. Sci.* 46 (2004) 109–135.
- [9] R. Davis, *Metals Handbook: Volume 13—Corrosion*, ninth edition, ASM International, Metals Park, Ohio, 1987.
- [10] S. Belkahl, H. Flores Zuñiga, G. Guenin, Elaboration and characterization of new low temperature shape memory Cu–Al–Be alloys, *Mater. Sci. Eng. A* 169 (1993) 119–124.
- [11] A. Hautcoeur, A. Eberhardt, E. Patoor, M. Berveiller, Thermomechanical behaviour of monocrystalline Cu–Al–Be shape memory alloys and determination of the metastable phase diagram, *J. Phys. IV C2* 5 (1995) 459–464.
- [12] S.N. Balo, M. Ceylan, M. Aksoy, Effects of deformation on the microstructure of a Cu–Al–Be shape memory alloy, *Mater. Sci. Eng. A* 311 (2001) 151–156.
- [13] S. Montecinos, A. Cuniberti, Aplicación de aleaciones con memoria de forma CuAlBe en amortiguamiento pasivo de estructuras civiles, *Revista SAM* 6 (3) (2009) 20–29.
- [14] S. Kustov, J. Pons, E. Cesari, M. Morin, J. Van Humbeeck, Athermal stabilization of Cu–Al–Be  $\beta'$  martensite due to plastic deformation and heat treatment, *Mater. Sci. Eng. A* 373 (2004) 328–338.
- [15] S. Montecinos, A. Cuniberti, Thermomechanical behavior of a CuAlBe shape memory alloy, *J. Alloys Compd.* 457 (2008) 332–336.
- [16] B. Kaouache, S. Berveiller, K. Inal, A. Eberhardt, E. Patoor, Stress analysis of martensitic transformation in Cu–Al–Be polycrystalline and single-crystalline shape memory alloy, *Mater. Sci. Eng. A* 378 (2004) 232–237.
- [17] S. Montecinos, A. Cuniberti, M.L. Castro, R. Boeri, Phase transformations during continuous cooling of polycrystalline  $\beta$ -CuAlBe alloys, *J. Alloys Compd.* 467 (2009) 278–283.
- [18] P.R. Swann, H. Warlimont, The electron metallography and crystallography of copper–aluminium martensites, *Acta Metall.* 11 (1963) 511–527.
- [19] X.J. Liu, I. Ohnuma, R. Kainuma, K. Ishida, Phase equilibria in the Cu-rich portion of the Cu–Al binary system, *J. Alloys Compd.* 264 (1998) 201–208.
- [20] A. Cuniberti, S. Montecinos, F.C. Lovey, Effect of  $\gamma_2$ -phase precipitates on the martensitic transformation of a  $\beta$ -CuAlBe shape memory alloy, *Intermetallics* 17 (2009) 435–440.
- [21] G.C. Serra, A.V. Benedetti, R.D. Noce, Electrochemical behavior of Cu–9%Al–5%Ni–2%Mn alloy in chloride media, *J. Braz. Chem. Soc.* 21 (8) (2010) 1530–1536.
- [22] G. Niaura, Surface-enhanced Raman spectroscopic observation of two kinds of adsorbed  $\text{OH}^-$  ions at copper electrode, *Electrochim. Acta* 45 (2000) 3507–3519.
- [23] S.T. Mayer, R.H. Muller, An in situ Raman spectroscopy study of the anodic oxidation of copper in alkaline media, *J. Electrochem. Soc.* 139 (1992) 426–434.
- [24] Raman Spectroscopic Library of the National Institute of Advances Industrial Science and Technology (AIST), <http://riodb.iase.aist.go.jp/riohomee.html> (last accessed: 30/08/2010).
- [25] M.L. Castro, R. Romero, Isothermal decomposition of the Cu–22.72Al–3.55Be at.% alloy, *Mater. Sci. Eng. A* 287 (2000) 66–71.
- [26] Agilent Technologies, [www.afm.university.org](http://www.afm.university.org) (last accessed: 30/08/2010).